




# Structural analytical and electrical conduction mechanisms of 2,7,12,17-tetra-*tert*-butyl-5,10,15,20-tetraaza-21*H*,23*H*-porphine nanostructure films

Ameen A. Al-Zubaidi<sup>1</sup>, Amel Abdallah Ahmed Elfaki<sup>1</sup>, S. A. Al-Ghamdi<sup>2,3</sup>, and A. A. A. Darwish<sup>3,4,5,\*</sup> 

<sup>1</sup>Department of Physics, Faculty of Science, Sudan University of Science and Technology, Khartoum, Sudan

<sup>2</sup>Department of Physics, Faculty of Science, University of Tabuk, 71491 Tabuk, Saudi Arabia

<sup>3</sup>Renewable Energy & Energy Efficiency Center, University of Tabuk, 71491 Tabuk, Saudi Arabia

<sup>4</sup>Department of Physics and Nanotechnology Research Unit, Faculty of Science, University of Tabuk, 71491 Tabuk, Saudi Arabia

<sup>5</sup>Department of Physics, Faculty of Education at Al-Mahweet, Sana'a University, Al-Mahweet, Yemen

Received: 5 January 2021

Accepted: 2 March 2021

Published online:

17 March 2021

© The Author(s), under exclusive licence to Springer Science+Business Media, LLC, part of Springer Nature 2021

## ABSTRACT

The 2,7,12,17-tetra-*tert*-butyl 5,10,15,20-tetraaza-21,23*H*-porphine (TTBTP) films were prepared using thermal evaporation technique. The X-ray diffraction (XRD) of the powder showed that TTBTP is polycrystalline with a tetragonal system. Also, the analysis of XRD pattern shows that the TTBTP film of thickness 55 nm has a crystallite size of 24.69 nm which tends to increase with the film thickness. By SEM of 177 nm thick TTBTP film, the topography of the surface is characterized by significant spherical granules. The mean diameter was estimated to be 250 nm for the spherical granules. It was observed that the conductivity increases with increasing the film thickness. Also, the TTBTP is a semiconductor film with thermally activated conduction mechanisms. The current–density–voltage (*J*–*V*) characteristics showed Ohmic drives in low voltage, whereas the space charge limited conductivity mechanism is familiar in the high voltage region. The carrier mobility values of TTBTP film are relatively the same for other organic molecules. The 50 nm TTBTP film has a carrier mobility of  $1.48 \times 10^{-9} \text{ cm}^2 \text{ V}^{-1} \text{ s}^{-1}$ , which increases with increasing the film thickness.

## 1 Introduction

The technology currently available derives from the unique physical properties of materials, such as abrasive surfaces, semiconductors, and magnets

[1–6]. Many of these materials exist in bulk, but reducing the material dimensions like thin films will lead to additional physical properties [7, 8]. Organic compounds are a recent field of electronic materials considered low-cost organic electronics prospects

Address correspondence to E-mail: [aaadarwish@gmail.com](mailto:aaadarwish@gmail.com)

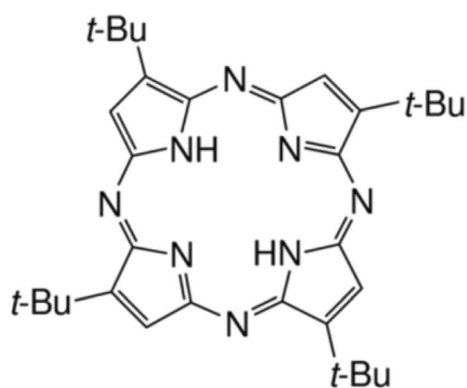
[9, 10]. At present, an expanding and dynamic field of research is the study of organic semiconducting materials. Mainly for their physical properties (optical, electrical, etc.), a variety of applications can be envisaged, such as Schottky diodes [11], photovoltaic devices [12], transistors for field effects [13], light-emitting diodes [14], and gas sensors [15].

Porphyrin dyes play a significant role in many biological processes, from the transport of oxygen to photosynthesis, from catalysts to improvements in pigmentation and optoelectronics and laser processing to electronics [15–18] and have received significant attention in the research community [15–20]. One of the Porphyrin family is 2,7,12,17-Tetra-*tert*-butyl-5,10,15,20-tetraaza-21*H*,23*H*-porphine (TTBTP), which is a molecular organic semiconductor grown in very ordered thin films, and currently under investigation as the principal thin film candidate [21].

In the previous work on TTBTP thin films, TTBTP films were found to have band gaps of 1.75 eV, making these films appropriate for optoelectronic applications [21]. Therefore, this work deals with investigating the structural and electrical properties of TTBTP films and calculating the essential parameters that give the possibility of applying it in manufacturing heterojunction devices. One particular aspect is film thickness, and it affects the electrical and magnetic properties and requires a precise characterization.

## 2 Experimental

The organic compound, TTBTP, was purchased from Sigma-Aldrich (see Scheme 1). TTBTP has the empirical formula,  $C_{32}H_{42}N_8$ , and a molecular weight



**Scheme 1** The molecular structure of the TTBTP compound

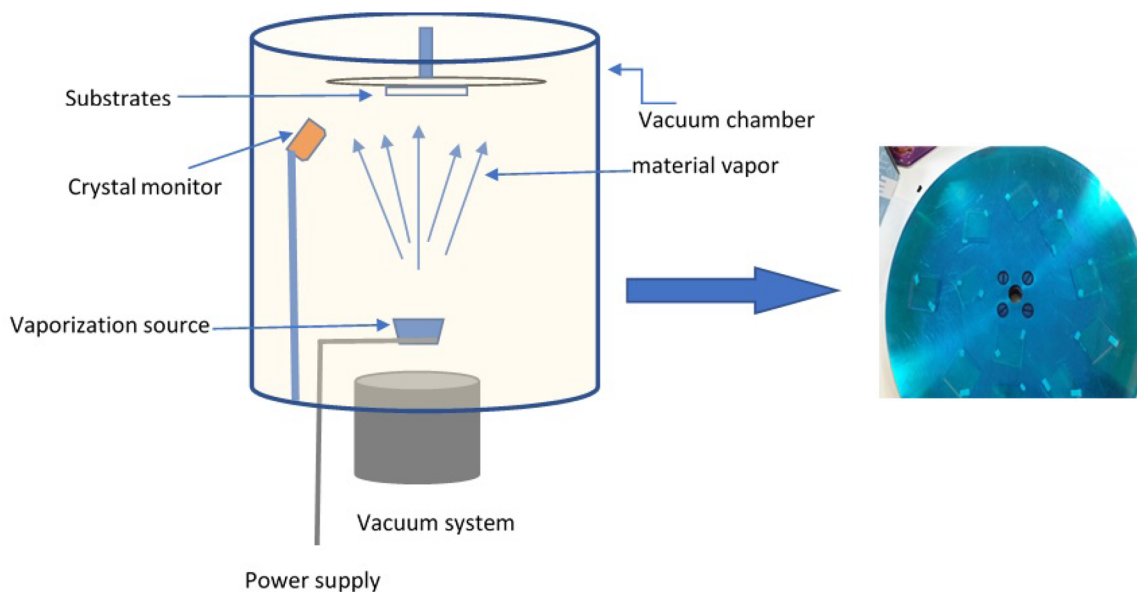
of 538.73 g/mol. TTBTP films of varying thicknesses (50, 95, 133, and 177 nm) were obtained by employing the efficient thermal vacuum evaporation technique. Using a coating unit (HHV Auto 306), the vacuum chamber was evacuated for 4 h. The thermal evaporation procedure is shown in Scheme 2. The pressure was  $1.32 \times 10^{-4}$  Pa to avoid the evaporated powder's interaction with the remaining impure gases. The TTBTP vapor subsequently was deposited into a cleaned glass substrate. The layer's deposition rate was 1.25 nm/s, while a quartz crystal monitor controlled the film thickness. Then, the thickness of the film was analyzed using an interferometric method. The films were prepared in a planar configuration for the measurement of electrical conductivity. While a sandwich configuration Au/TTBTP/Au for  $J$ - $V$  measurements. Au electrodes were evaporated over the prepared films via a mask.

In this study, the structure of TTBTP in powder and thin film form has been investigated and characterized by X-ray diffraction (XRD). This test was achieved by a modern automated and computer-based (Philips X'pert) diffractometer with  $CuK\alpha$  Ni-filtered radiation ( $\lambda = 0.1542$  nm), operated at 35 kV and 30 mA. In surface morphology, an electron microscope platform SEM-Joel has been used to scanning electron microscope (SEM) images for TTBTP films. Using a digital electrometer (Keithley model 610), the electrical resistance ( $R$ ) was calculated. The electrical conductivity ( $\sigma$ ) was calculated using the equation  $\sigma = L/RA$ , where  $L$  refers to the length, and  $A$  refers to the area. For  $J$ - $V$  measurements, a sandwich configuration of the Au/TTBTP/Au was accomplished. As a source of current and a meter, a Keithley Model 617 with a high impedance electrometer was used to test current at different voltages. The sample temperature was evaluated by a Cr–Al thermocouple, monitored by a micro-voltmeter.

## 3 Results and discussion

### 3.1 Structural investigation

The structure of TTBTP material was measured by X-ray diffraction (XRD) patterns at room temperature. Figure 1 displays TTBTP powder XRD patterns in a polycrystalline structure. For all diffraction lines, the lattice parameters were determined using the



**Scheme 2** The schematic diagram of the thermal evaporation process

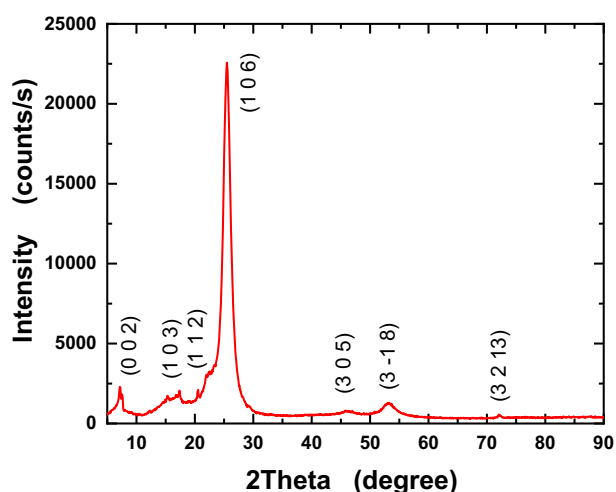


**Fig. 1** XRD pattern of TTBTTP compound in the powder form

CRYSFIRE program [22]. The results obtained showed that the TTBTTP crystal system is tetragonal with group space P42. The lattice parameters were given as  $a = b = 6.507$  nm,  $c = 24.832$  nm, and  $\alpha = \beta = \gamma = 90^\circ$ . The CHECKCELL program was used to calculate the Miller indices ( $hkl$ ) for each diffraction peak [23]. Table 1 shows the values of the Miller indices ( $hkl$ ) and the interplanar spacing ( $d_{hkl}$ ) for each diffraction peak.

Figure 2 displays the XRD pattern for TTBTTP films at different film thicknesses. This figure reveals that the rise in film thickness is affecting rising film crystallography. There is only one significant peak in

the (3 0 5) direction indicating preferential orientation. Also, the increase in the crystallinity of films can be deduced by the increase in thickness due to the rise of aggregation particles as the deposited layers of the TTBTTP material increase [24].

Commonly, film nanostructure can be examined by evaluating the mean size of crystallite ( $D$ ). Based on Scherrer's equation, the following expression can be used to test the  $D$  values [25]:

$$D = \frac{K\lambda}{\beta \cos \theta}, \quad (1)$$

where  $K$  is the Scherrer's constant,  $\lambda$  is the X-ray wavelength ( $\lambda = 0.154$  nm), and  $\beta$  is the peak width (in radians) at the half-maximum. The values of  $D$  were calculated and increased in these values from 24 to 56 nm with the accretion of film thickness from 50 to 177 nm, respectively, as shown in Table 2. It can, therefore, be inferred that TTBTTP films exhibit nanostructure-based properties. Moreover, the enhancement of crystallography was observed with an increase in the film thickness.

It is also convenient to measure some useful crystalline parameters such as the density of dislocation, which indicates the length of dislocation lines per unit volume, the number of crystallites per unit surface area ( $N_c$ ), and the density of dislocation ( $\epsilon_s$ ). Those parameters could be assessed from the following terms [26]:

**Table 1** The interplanar spacing ( $d_{hkl}$ ) and the values of Miller indices  $h k l$  for TTBT powder

No.	$2\theta$ (°)		$d$ (nm)		$I/I_0$	$h$	$k$	$l$
	Observed	Calculated	Observed	Calculated				
1	7.18	7.11	12.51	12.42	10.17	0	0	2
2	17.38	17.32	5.14	5.12	9.13	1	0	3
3	20.56	20.57	4.28	4.31	9.33	1	1	2
4	25.48	25.49	3.49	3.49	100	1	0	6
5	45.70	45.60	2.01	1.99	3.56	3	0	5
6	53.32	53.38	1.69	1.72	5.73	3	-1	8
7	72.04	71.92	1.38	1.31	2.48	3	2	13

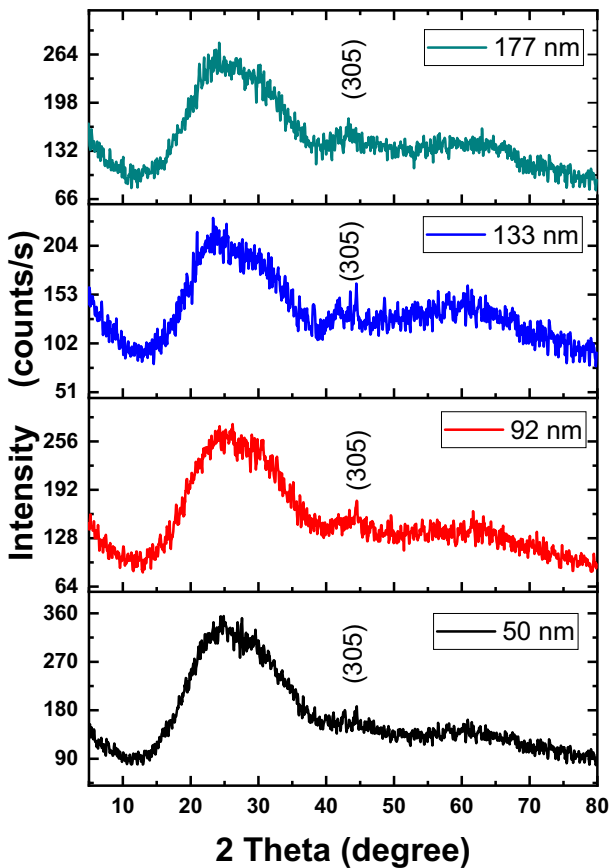


**Fig. 2** XRD of TTBT films with different thicknesses

**Table 2** Crystalline parameters of TTBT with different thicknesses

$d$ (nm)	$D$ (nm)	$\delta \times 10^{10}$ (line $\text{cm}^{-2}$ )	$\epsilon_s \times 10^{-4}$	$N \times 10^{10}$ ( $\text{cm}^{-2}$ )
50	24.69	16.41	14.82	61.16
92	27.76	12.47	13.17	62.14
133	54.52	3.36	6.71	10.93
177	56.08	3.18	6.52	2.84

$$\delta = \frac{1}{D^2}, \tag{2}$$

$$N_c = \frac{d}{D^3}, \tag{3}$$

$$\epsilon_s = \frac{\beta \cos \theta}{4}, \tag{4}$$

where  $d$  refers to the film thickness. The corresponding values of  $\delta$ ,  $N_c$  and  $\epsilon_s$  for various film thicknesses were presented in Table 2. Contrary to the rise in  $D$  value as the film increases, it was found that the values of  $\delta$ ,  $N_c$  and  $\epsilon_s$  decrease. This decrease provides evidence of the defects and imperfections reduction as the film thickness increases.

SEM can provide good surface renditions, but specimens need to be vacuum-coated with gold to avoid charging. SEM was used to study the TTBT film morphologies. Figure 3 exhibits the morphologies of 177 nm thick TTBT films. The topography of the surface, as shown, is distinguished by significant spherical granules. The particle diameter analysis histogram is shown in Fig. 4, accomplished with the well-known online software IMAGE J. The value of the mean diameter of the spherical granules was estimated to be about 250 nm, which was taken from the histogram.

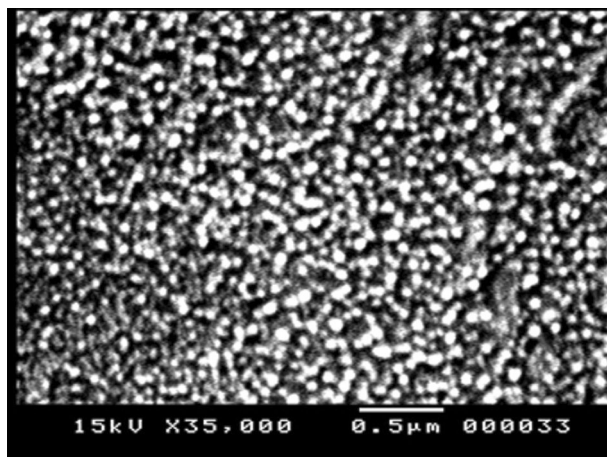


**Fig. 3** SEM of TTBTB films with thicknesses of 177 nm

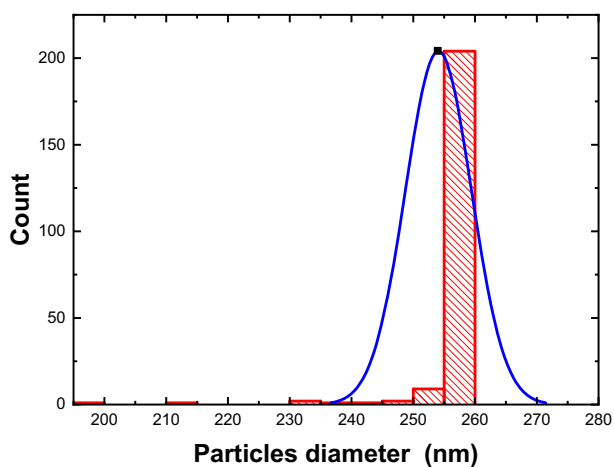


**Fig. 4** Distributinal histogram of TTBTB particle size deduced from the SEM image

### 3.2 Electrical conductivity investigation

The electrical conductivity ( $\sigma$ ) in the material gives an insight into the carrier-charging mechanism. One of the notable points in the conduction analysis is the measured thermal activation energy of the materials. Figure 5 depicts the relation between  $\ln\sigma$  and  $1000/T$  for TTBTB film with different thicknesses. This figure shows the increase in conductivity with the film's thickness because the structural crystalline is improved, and the grain size's productivity within the material increases [27] (Table 3).

Figure 5 indicates that the TTBTB film is a semiconductor with two thermally activated conduction mechanisms. This behavior implies that  $\ln(\sigma)$  has direct proportional to  $1000/T$ , according to Arrhenius [28]:

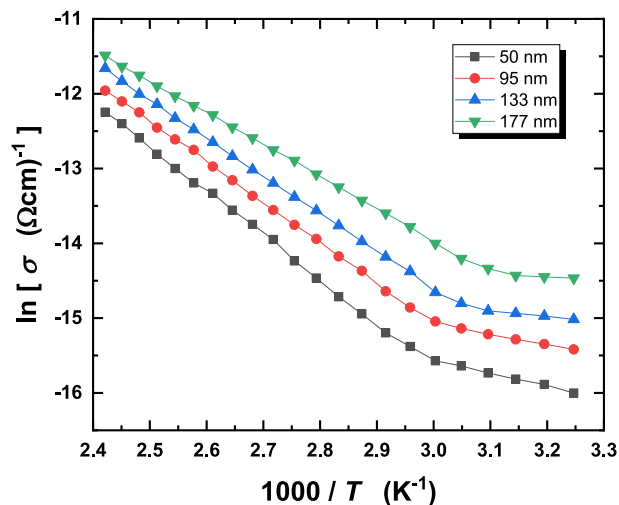


**Fig. 5** The relation between  $\ln\sigma$  and  $1000/T$  for TTBTB films with different thicknesses

$$\sigma = \sigma_{o1} \exp\left(\frac{-\Delta E_1}{k_B T}\right) + \sigma_{o2} \exp\left(\frac{-\Delta E_2}{k_B T}\right), \quad (5)$$

where  $k_B$  is the Boltzmann constant. The pre-exponential factors are  $\sigma_{o1}$  as well as  $\sigma_{o2}$ . In regions (I) and (II), the electrical activation energy is  $\Delta E_1$  and  $\Delta E_2$ , respectively. These parameters were calculated and listed in Table 4. The  $\Delta E$  values of TTBTB films were found to be in the same order as other related organic semiconductors [28, 29]. Therefore, the conductivity mechanism is extrinsic conduct in the region (I), while the mechanism is intrinsic in the region (II). Further, Table 4 demonstrates the decrease in  $\Delta E$  and  $\sigma_o$  values with rising film thickness. Therefore, the activation energy indicates the charges' energy to move between the localized states' two locations. Thus, the growth of the deposited layers has a distinct impact on the recovery process, decreasing both the degree of disorder and the defects caused within the sample. These observations align with the XRD study.

### 3.3 Current–density–voltage investigation

The space charge limited conductivity (SCLC) and the Ohmic electrical investigation are further illuminating the charging mechanism and the trapping of carriers in the material. The current–density–voltage ( $J$ – $V$ ) characteristics for the structure for sandwiches of TTBTB film at different film thicknesses are shown in Fig. 6, which clarifies two various conducting fields, each with a threshold voltage and two



**Table 3** Electrical parameters of TTBTTP with different thicknesses

<i>d</i> (nm)	High temperature		Low temperature	
	$\sigma_{o1}$ ( $\Omega\text{ cm}$ ) <sup>-1</sup>	$\Delta E_1$ (eV)	$\sigma_{o2}$ ( $\Omega\text{ cm}$ ) <sup>-1</sup>	$\Delta E_1$ (eV)
50	9.15	0.51 ± 0.04	33.06 × 10 <sup>-6</sup>	0.151 ± 0.02
92	3.23	0.46 ± 0.04	18.73 × 10 <sup>-6</sup>	0.120 ± 0.01
133	1.63	0.43 ± 0.04	4.71 × 10 <sup>-6</sup>	0.073 ± 0.01
177	0.29	0.36 ± 0.04	3.29 × 10 <sup>-6</sup>	0.048 ± 0.02

**Table 4** SCLC parameters of TTBTTP with different thicknesses

<i>d</i> (nm)	Ohmic region		SCLC region	
	$E_F$ (eV)	$\mu$ (10 <sup>-9</sup> cm <sup>2</sup> V <sup>-1</sup> S <sup>-1</sup> )	$E_t$ (eV)	$N_t$ (cm <sup>-3</sup> )
50	0.59 ± 0.02	1.48	0.41 ± 0.02	2.05 × 10 <sup>18</sup>
92	0.62 ± 0.02	2.84	0.35 ± 0.02	1.46 × 10 <sup>17</sup>
133	0.66 ± 0.01	7.22	0.31 ± 0.01	6.68 × 10 <sup>16</sup>
177	0.69 ± 0.02	18.96	0.26 ± 0.02	6.34 × 10 <sup>16</sup>

different slopes. The slope was determined to be 1.04 ± 0.02 in the first region. The calculated slope was found to be about 2.02 ± 0.05 concerning the second region. In low voltage, particularly the disappearance of charge traps into the forbidden gap is characterized by the disappearance, and it is known as the Ohmic drives. In contrast, the SCLC drive mechanism is familiar in the high voltage region [30].

Figure 7 shows the variation of ln *J* versus 1000/*T* for TTBTTP at different film thicknesses in Ohmic areas. The interpretation of *J* to *V* for p-type material in the Ohmic domain can be explained in the following equation [31].

$$J = N_{oq}\mu(V/d)\exp(-E_F/kT), \tag{6}$$

where *N<sub>o</sub>* is the effective density of states in the valence band, which is found to be 10<sup>21</sup> cm<sup>3</sup> [32], *q* is the charge of the carriers,  $\mu$  is the carrier’s mobility, and *E<sub>F</sub>* is the Fermi-energy level. In the Ohmic region; therefore, *E<sub>F</sub>* values can be determined to employ the slope of the fitting line, whereas the  $\mu$  values can be evaluated from the crossroads between the line and the ln*J* axis of different film thicknesses, the values of *E<sub>F</sub>* and  $\mu$  of TTBTTP films are given in Table 4. The values of  $\mu$  reveal that the carrier’s mobility of this material is relatively the same order as other organic

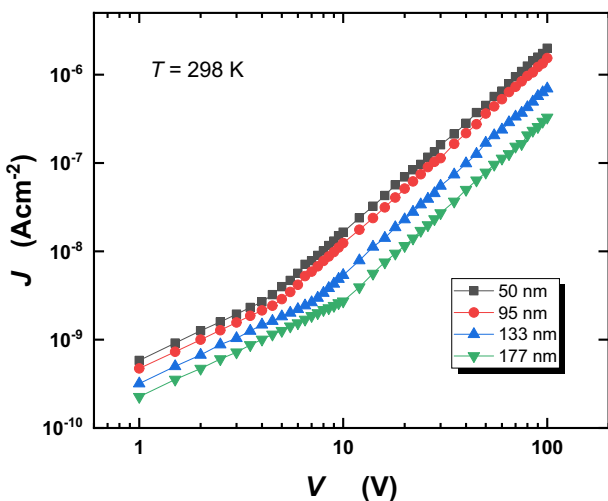


**Fig. 6** *J*-*V* characteristics Al/TTBTTP/Al sandwich structures of different thicknesses

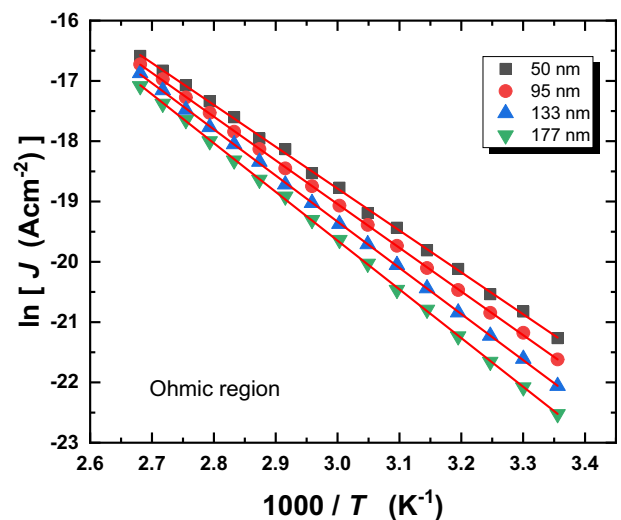


**Fig. 7** The relation between ln *J* and 1000/*T* for TTBTTP films in the Ohmic region

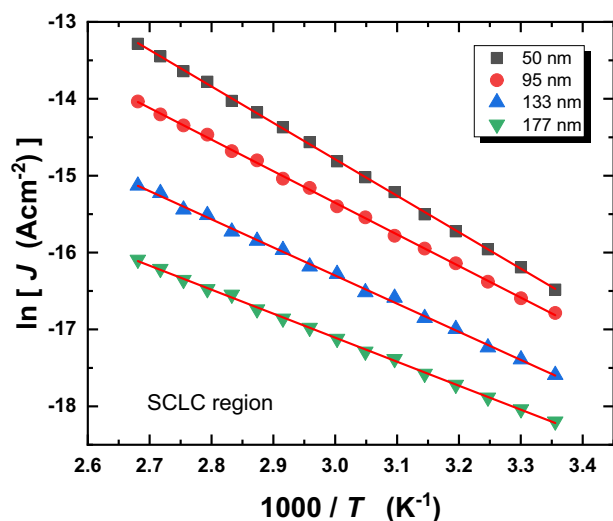


**Fig. 8** The relation between  $\ln J$  and  $1000/T$  for TTBTTP films in the SCLC region

molecules. For example, the  $\mu$  value of *N,N*-dimethyl-3,4,9,10-perylene-dicarboximide films, at the room temperature, was found to be  $7.21 \times 10^{-9} \text{ cm}^2 \text{ V}^{-1} \text{ s}^{-1}$  [33], whereas it was recorded to be  $1.56 \times 10^{-10} \text{ cm}^2 \text{ V}^{-1} \text{ s}^{-1}$  for films of 2,9-Bis [2-(4-2chlorophenyl)ethyl] anthrac [2,1,9-def:6,5,10-def'] diisoquinoline-1,3,8,10 (2*H*,9*H*) tetrone [34].

However, the relation  $\ln J$  versus  $1000/T$  in the SCLC region, which is shown in Fig. 8, can be evaluated by the following equation [31]

$$J = \frac{9}{8} \left( \frac{V^2}{d^3} \right) \left( \frac{N_0}{N_t} \right) \epsilon_0 \epsilon \mu \exp \left( \frac{-E_t}{k_B T} \right), \quad (7)$$

where  $N_t$  is the trap concentration and  $E_t$  refers to the trap energy level above the valence band's edge. The permittivity for free space is  $\epsilon_0$ , and the dielectric constant of the film TTBTTP is  $\epsilon$ , which is given in the previous research for different thicknesses [21]. The parameters  $N_t$  and  $E_t$  were calculated and listed in Table 4. It was concluded that the  $N_t$  value of the present sample is compatible with the other organic molecules. On the other hand, the trap concentration decreases with raising the film thickens due to reducing both the degree of disorder and the defects.

## 4 Conclusions

X-ray powder diffraction TTBTTP powder showed its polycrystallinity with a tetragonal orientation. Thermal evaporation of TTBTTP led to nanocrystalline

films oriented preferentially to the (3 0 5) plane with an amorphous background. The crystalline size increased by film thickens. However, the SEM of TTBTTP film shows the film's uniform formation and indicates nanocrystalline structure formation. The mean diameter value of the spherical granules was estimated to be about 250 nm. In TTBTTP films, the electrical conductance temperature reliance suggests that the conduction is activated by a thermal cycle. The calculated values for both  $\Delta E$  and  $\sigma_0$  show that electric conduct is extrinsic conduct followed by intrinsic. Measurements of current density as a function of temperature allowed the estimation of mean mobility values and trap concentration from SCLC data. The mobility values increase as the film increases, and it was comparable with other organic molecules. This result makes the TTBTTP compounds promising materials for use in a wide variety of optoelectronic applications.

## References

1. L.I. Maissel, R. Glang, *Handbook of Thin Film Technology* (McGrawHill, New York, 1980).
2. M. Ohring, *The Material Science of Thin Films* (Academic Press, San Diego, 1992).
3. Z.-R. Jia, Z.-G. Gao, Y.-H. Di Lan, G.-L. Cheng, Wu, H.-J. Wu, Effects of filler loading and surface modification on electrical and thermal properties of epoxy/montmorillonite composite. *Chin. Phys. B* **27**, 117806 (2018)
4. S. Chen, G. Meng, B. Kong, B. Xiao, Z. Wang, Z. Jing, Y. Gao, G. Wu, H. Wang, Y. Cheng, Asymmetric alicyclic amine-polyether amine molecular chain structure for improved energy storage density of high-temperature cross-linked polymer capacitor. *Chem. Eng. J.* **387**, 123662 (2020)
5. K. Yiqun Wang, G. Kou, A. Wu, Feng, L. Zhuo, The effect of bis allyl benzoxazine on the thermal, mechanical and dielectric properties of bismaleimide-cyanate blend polymers. *RSC Adv.* **5**, 58821–58831 (2015)
6. K. Yiqun Wang, G. Kou, L. Wu, J. Zhuo, Yu Li, Zhang, The curing reaction of benzoxazine with bismaleimide/cyanate ester resin and the properties of the terpolymer. *Polymer* **77**, 354–360 (2015)
7. L.B. Freund, S. Suresh, *Thin Film Materials* (Cambridge University Press, Cambridge, 2003).
8. D. Smith, *Thin Film Deposition: Principles and Practice* (McGrawHill, New York, 1995).

9. D. Ji, T. Li, H. Fuchs, Patterning and applications of nanoporous structures in organic electronics. *Nano Today* **31**, 100843 (2020)
10. N.A. Azarova, J.W. Owen, C.A. McLellan, M.A. Griminger, E.K. Chapman, J.E. Anthony, O.D. Jurchescu, Fabrication of organic thin-film transistors by spray-deposition for low-cost, large-area electronics. *Org. Electron.* **11**, 1960–1965 (2010)
11. V. Chaudhary, N. Kumar, A.K. Singh, Solubility dependent trap density in poly (3-hexylthiophene) organic Schottky diodes at room temperature. *Synth. Met.* **250**, 88–93 (2019)
12. Y. Xia, X. Xu, O. Inganäs, Photovoltage loss in semi-transparent organic photovoltaic devices. *Org. Electron.* **74**, 37–40 (2019)
13. D.K. Kim, J.-Ho. Choi, A study of effects of electrode contacts on performance of organic-based light-emitting field-effect transistors. *Opt. Mater.* **76**, 359–367 (2018)
14. L. Wang, Metal-organic frameworks for QCM-based gas sensors: a review. *Sensors Actuators A* **3071**, 111984 (2020)
15. Y.G. Mourzina, A. Offenhäuser, Electrochemical properties and biomimetic activity of water-soluble meso-substituted Mn(III) porphyrin complexes in the electrocatalytic reduction of hydrogen peroxide. *J. Electroanal. Chem.* **8661**, 114159 (2020)
16. R. Boukoureshtlieva, Y. Milusheva, I. Popov, A. Trifonova, A. Momchilov, Application of pyrolyzed Cobalt(II) tetramethoxyphenyl porphyrin based catalyst in metal-air systems and enzyme electrodes. *Electrochim. Acta* **3531**, 136472 (2020)
17. G. Zhu, Q. Sun, Y. Kawazoe, P. Jena, Porphyrin-based porous sheet: optoelectronic properties and hydrogen storage. *Int. J. Hydrogen Energy* **40**, 3689–3696 (2015)
18. I. Sebarchievici, B.-O. Taranu, S.F. Rus, E. Fagadar-Cosma, Electrochemical behaviour and analytical applications of a manganese porphyrin-silica hybrid film prepared by pulsed laser deposition. *J. Electroanal. Chem.* **86515**, 114127 (2020)
19. M.M. El-Nahass, H.M. Zeyada, M.S. Aziz, M.M. Makhlof, Influence of high-energy X-ray irradiation on the optical properties of tetraphenylporphyrin thin films. *Opt. Laser Technol.* **39**, 347–352 (2007)
20. H.M. Zeyada, M.M. El-Nahass, M.M. Makhlof, Electronic transport mechanisms in tetraphenyleprophyrin thin films. *Curr. Appl. Phys.* **11**, 1326–1331 (2011)
21. A.A. Al-Zubaidi, A.A.A. Elfaki, A.A.A. Darwish, Influence of film thickness on structural and optical properties of 2,7,12,17-tetra-*tert*-butyl-5,10,15,20-tetraaza-21*H*,23*H*-porphine nanostructure thin films for optical applications. *J. Mol. Struct.* **1218**, 128499 (2020)
22. R. Shirley, *The CRYSFIRE System for Automatic Powder Indexing: User's Manual* (The Lattice Press, Guildford, 2000).
23. J. Laugier, B. Bochu, Checkcell, LMGP-Suite of Programs for the Interpretation of X-Ray Experiments. Ensp/Laboratoire des Materiaux et du Genie, Physique, Saint Martin d'Herès (2004)
24. A.Z. Mahmoud, A.A.A. Darwish, S.I. Qashou, Film thickness effects on nanorods organic films of azo quinoline derivatives for optical. *Progress Natural Sci.* **29**, 402–409 (2019)
25. I. Saleem, S.E. Qashou, A.A.A. Al Gami, M.M. Darwish, A. Hawamdeh, Aldrabee, **Gamma radiation effect on physical properties of 2,9-Bis [2-(4-chlorophenyl)ethyl] anthrax [2,1,9-def:6,5,10-d'e'f'] diisoquinoline-1,3,8,10 (2H,9H) tetrone films**, *Optik* **170** (2018) 540–547
26. S. Venkatachalam, D. Mangalaraj, S.K. Narayanadass, Characterization of vacuum evaporated ZnSe thin films. *Phys. B* **393**, 47–55 (2007)
27. A.R. Bushroa, R.G. Rahbari, H.H. Masjuki, M.R. Muhamad, Approximation of crystallite size and microstrain via XRD line broadening analysis in TiSiN thin films. *Ultrason. Sonochem.* **86**, 1107–1112 (2012)
28. M.M. El-Nahass, K.F. Abd-El-Rahman, A.A.A. Darwish, Electrical conductivity of 4-tricyanovinyl-*N,N*-diethylaniline. *Phys. B* **403**, 219–223 (2008)
29. K.N.N. Unni, C.S. Menon, Electrical and optical studies on metal-free phthalocyanine thin films. *J. Mater. Sci. Lett.* **20**, 1207–1209 (2001)
30. M.A. Lampert, P. Mark, *Current Injection in Solids* (Academic Press, New York, 1970).
31. A. Ahmad, R.A. Collins, Ohmic and space-charge-limited conduction in lead phthalocyanine thin films. *Phys. Status Solidi A* **123**, 201 (1991)
32. R.D. Gould, The interpretation of space-charge-limited currents in semiconductors and insulators. *J. Appl. Phys.* **53**, 3353 (1982)
33. I. Saleem, A.A.A. Qashou, S.E. Darwish, Al Gami, Enhancement of microstructure and electrical conductivity of *N,N'*-dimethyl-3,4,9,10-perylenedicarboximidenanostructured films by thermal annealing for photoelectronic applications. *Synth. Met.* **242**, 67–72 (2018)
34. A.A.A. Darwish, E.F.M. El-Zaidia, S.I. Qashou, **Investigation of structural and electrical properties of 2,9-Bis [2-(4-chlorophenyl)ethyl] anthrax [2,1,9-def:6,5,10-d'e'f'] diisoquinoline-1,3,8,10 (2H,9H) tetrone (Ch-diisoQ) nanostructured films for photoelectronic applications**, *Physica B* **558** (2019) 116–121

**Publisher's Note** Springer Nature remains neutral with regard to jurisdictional claims in published maps and institutional affiliations.